Monte Carlo Simulation of Electron Transport in wurtzite Indium Nitride

C.SAYAH*, B.BOUAZZA**, A.GUEN-BOUAZZA, N.E.CHABANE-SARI

Unité de Recherche Matériaux et Energies Renouvelables, Faculté de Technologie,
Université Abou-Bekr Belkaïd de Tlemcen.BP 230, Tlemcen 13000, Algérie.

ABSTRACT

Among the group-III nitrides, InN displays markedly unusual electronic transport characteristics due to its smaller effective mass, high peak velocity and high background electron concentration. We present the steady-state, velocity-field characteristics of wurtzite indium nitride, determined using an ensemble Monte Carlo approach. A three valley model for the conduction band is employed and ionized impurity, polar and non polar optical phonon, acoustic deformation potential, piezoelectric, deformation potential and intervalley scattering mechanisms are considered. The sensitivity of these steady-state results to variations in temperature and doping concentration is examined. Our results suggest that the transport characteristics of indium nitride are superior to those of gallium nitride and gallium arsenide, over a wide range of temperatures, from 77 to $600\,K$, and doping concentrations, up to $1.0x10^{19}\,cm^{-3}$. Hence, indium nitride has considerable potential for device applications.

Keywords- Monte Carlo method, semiconductor materials, wide bandgap semiconductors.

I. INTRODUCTION

The III-nitride-based systems in general and InN in particular have attracted a great deal of attention in recent years. These materials had been known to have wide band-gap energies ($3.42\,eV$ for **GaN**, $6.2\,eV$ for **AlN**, and $1.89\,eV$ for **InN**) so that they can be used for the fabrication of devices working in the blue and ultraviolet regions of the spectrum. However, there is controversy over the material parameters of InN and, according to recent studies, its band gap value is between $0.7\,eV$ and $0.8\,eV$ [1,2] with band-gap bowing of $1.43\,eV$ [3] In addition to the intriguing controversy about the fundamental band gap of InN, another undetermined important parameter is the effective mass m*. Effective mass plays a dominant role for transport and mobility characteristics and device design but various values have been reported for InN. The commonly used, traditional value for the effective mass is $0.11m_e$ [4] but for the band gap of 0.7– $0.8\,eV$, the effective mass is presented as $0.07m_e$ [5] and in other studies as $0.042m_e$ [6,7], where m_e is the free electron mass. A more-recent study even questions the validity of a band-gap value of about $0.7\,eV$[8]. Previously commonly used parameter values for the band-gap energy, band-gap bowing, and effective mass for InN were $1.89\,eV$[9], $3.8\,eV$[10], and $0.11m_e$ [4], respectively. The electron transport characteristics of InN have been studied [11, 12] and during the past few years electron low-field mobilities in InN above 2000 $cm^2/V\,s$ have been measured [13, 14]. The best reported mobility of InN at room temperature was about $3500\,cm^2/V$ s [15]. Recent theoretical estimates for low-field mobility with undoped InN have reached about $14,000\,cm^2/V\,s$ at room temperature [16]. Among the III-nitride materials, InN exhibits the highest peak overshoot velocity when compared with GaN and AlN [17]. A more-recent study where the newly published material parameters for InN are used shows that the peak velocity of electrons in bulk InN increases significantly [18, 19].

Parameter	InN
Mass density (g/cm³)	6.81
Longitudinal sound velocity (cm/s)	6.24×10^5
Transverse sound velocity (cm/s)	2.55×10^5
Acoustic deformation potential (eV)	7.1
Static dielectric constant	15.3
High-frequency dielectric constant.	8.4
Effective mass (Γ_1 valley) [67]	$0.11\ m_e$
Piezoelectric constant, e_{14} (C/cm²)	3.75×10^{-5}
Direct energy gap (eV)	1.89
Optical phonon energy (meV)	89.0
Intervalley deformation potentials (eV/cm)	10^9
Intervalley phonon energies (meV)	89.0

Valley number		1	2	3		1	2	3
Valley location	InN 1	Γ_1	A	Γ_2	InN2	Γ_1	A	Γ_2
Valley degeneracy		1	1	1		1	1	1
Effective mass		$0.11\ m_e$	0.40	0.60		$0.11\ m_e$	m_e	m_e
Intervalley energy separation (eV)		-	2.2	2.6		-	2.2	2.6
Energy gap (eV)		1.89	0.088	0.036		1.89	4.09	4.49
Non-parabolicity (eV^{-1})		0.419	0.0	0.0		0.419	0.0	0.0

Table 1: Traditional parameter values for wurtzite InN.

Other attributes of III-nitride systems are that their energy gaps can be varied over a wide range and these systems have high electron mobilities and heat conductivities and in addition, for example, GaN has a high breakdown voltage and a small dielectric coefficient [4, 20, 21]. In the present work we study the low-field transport properties of wurtzite InN using Ensemble Monte Carlo simulation (EMC). A three-valley model for the conduction band is employed (**Table 1**) [22, 23]. The scattering mechanisms considered in our analysis are ionized impurity, polar and non polar optical phonon, acoustic deformation potential, piezoelectric and Intervalley scattering is also considered. We first analyse, in Section 2, the electronic transport properties of wurtzite InN. In particular, the velocity-field characteristic associated with this material will be examined in detail. Then, an overview of our steady-state electron transport results, corresponding to the three III-V nitride semiconductors under consideration in this analysis, will be given, and a comparison with the more conventional III-V compound semiconductor, GaAs, will be presented. A comparison between the temperature dependence of the velocity-field characteristics associated with wurtzite InN will then be presented, and our Monte Carlo results will be used to account for the differences in behavior. A similar analysis will be presented for the doping dependence. We also explore the sensitivity of the velocity-field characteristic associated with bulk wurtzite InN to variations in the band structure.

II. RESULTS AND DISCUSSION

In **Fig. 1**, the simulated electron drift velocity is plotted as function of applied electric field in wurtzite InN, these results being obtained from Monte Carlo simulations of electron transport at 300 K and electron concentration is equal to $10^{16}\ cm^{-3}$. We find that wurtzite InN achieves a peak drift velocity of about $\approx 3.8 \times 10^7\ cm/s$ at an electric field of around $68\ kV/cm$. At higher electric fields the drift velocity decreases, eventually saturating at around $1.5 \times 10^7\ cm/s$. In **Fig. 1**, we also plot the average energy of electrons in wurtzite InN as a function of the applied field. We find that with no applied field that the average electron energy is $3/2kT$. With increases in the applied field, however, the average electron energy remains small, of the order of the polar optical phonon energy, until the applied field exceeds 50 kV/cm, at which point the average electron energy increases clearly. This increase in the average energy continues until the intervalley energy separation is achieved, at which point many of the electrons will have transferred from the central valley to the upper valleys; the lowest energy upper conduction band valley minima in InN occur 2,60 eV above the conduction band valley minimum. These results suggest that polar optical phonon instability occurs in wurtzite InN and that this instability is responsible for the onset of intervalley transitions. In order to confirm that intervalley transitions begin when the applied field is around 50 kV/cm in InN at 300 K.
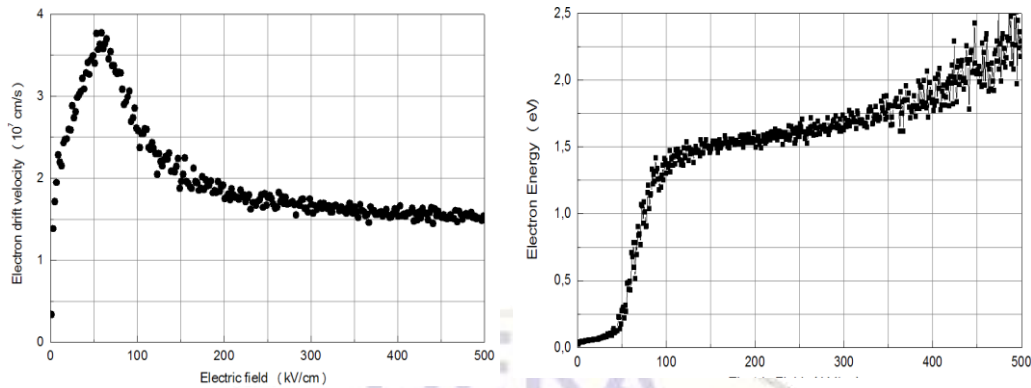
Fig.1. Steady state electron velocity and average energy as a function of electric field in wurtzite InN.

in **Fig. 2**, we also plot the fractional electron occupancy of the central conduction band valley as a function of the applied field for wurtzite InN at 300 K, these results being from Monte Carlo simulations of electron transport in this material. We see that intervalley transitions, as indicated by a decrease in the occupancy of the central valley, do indeed begin in the neighborhood of 50 kV/cm. As the applied electric field is increased, the average electron energy increases until a substantial fraction of the electrons have acquired enough energy in order to transfer into the upper valleys. As the effective mass of the electrons in the upper valleys is greater than that in the lowest valley, the electrons in the upper valleys will be slower. As more electrons transfer to the upper valleys, the electron drift velocity decreases. This accounts for the negative differential mobility observed in the velocity–field characteristic depicted in **Fig. 1**.
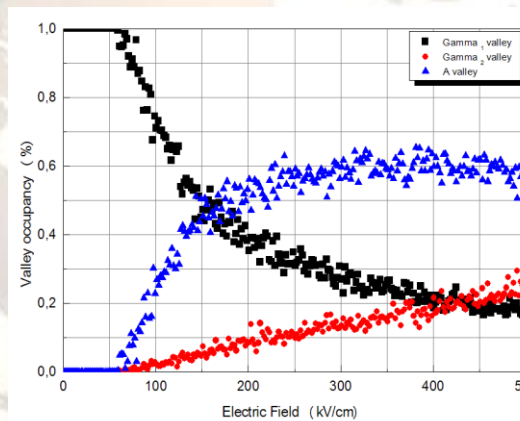

Fig.2. Fractional occupation of the central Γ_1 and satellite valleys of wurtzite InN as a function of applied electric field.

In **Fig. 3**, we plot the velocity-field characteristic associated with bulk wurtzite InN for which we will attempt to compare the transport properties when the traditional material parameters and the more-recent ones are used. For the traditional material parameter values of effective mass $0.11m_e$, gap energy $1.89\ eV$, and nonparabolicity value of $0.419\ eV^{-1}$ resulting from the Kane model, a highest velocity value of $3.8x10^7\ cm/s$ is attained at a field value of about $68\ kV/cm$ (labeled InN1-InN2 in **Fig. 3**). Let us now consider the case of new parameters for InN. When the newly suggested value of effective mass $0.07m0$, gap energy $0.8\ eV$, and the nonparabolicity factor of $1.081\ eV^{-1}$ corresponding to these values resulting from Kane model are used for InN, the peak velocity increases to a value of about $4.3x10^7\ cm/s$ and the field at which this value is attained decreases to about 50 kV/cm (labeled InN3 in **Fig. 3**).
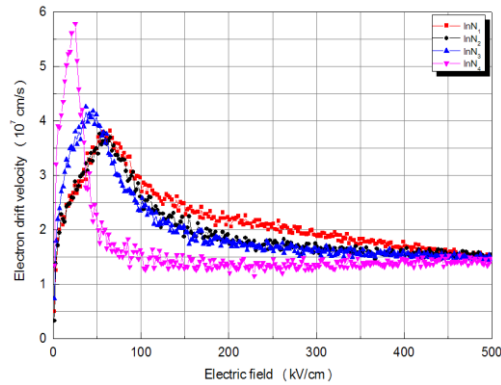
Fig.3. Velocity–field characteristic of electrons for wurtzite InN as a function of applied electric field.

Finally if one uses the other latest value of effective mass of $0.042m0$ with its corresponding nonparabolicity factor $1.147\ eV^{-1}$, the peak velocity increases to a value of about $5.9x10^7\ cm/s$ at an applied field of about $24\ kV/cm$ (labeled as InN4 in **Fig. 3**). This latter value is found to be $22.5\ kV/cm$ with a peak velocity of about $6x10^7\ cm/s$ by O'Leary et al. [18] However, their parameters are slightly different from the ones we have used in this study. In a similar Monte Carlo study by Ref. [22] the peak velocity is found to be $5.3 \cdot 10^7\ cm/s$ at a field value $32\ kV/cm$. Our results are more compatible with the latter study. The peak electron drift velocity, the saturation electron drift velocity, and the low field electron drift mobility associated with wurtzite InN are plotted as functions of the doping concentration in **Fig. 4**.
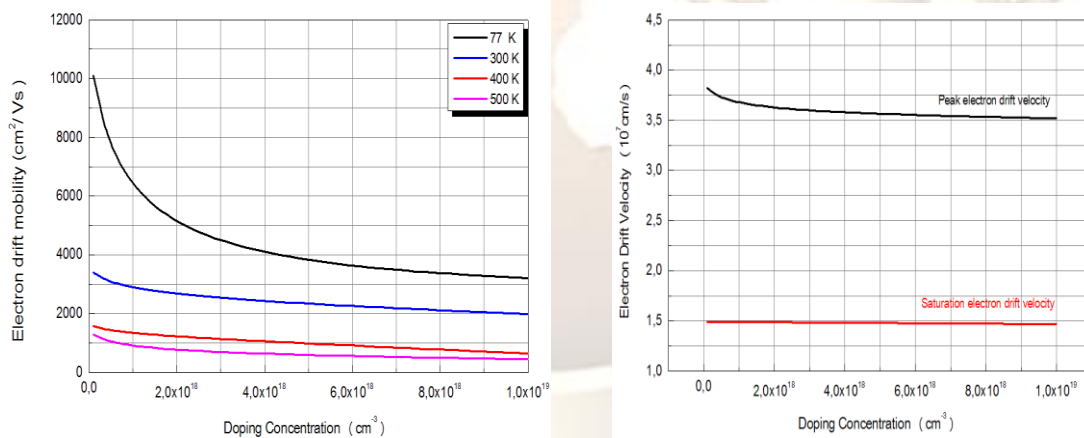
Fig.4. The low field electron drift mobility, the peak electron drift velocity and the saturation electron drift velocity associated with wurtzite InN as functions of the doping concentration

It is noted that for doping concentrations below $10^{16}\ cm^{-3}$, the velocity-field characteristic associated with InN exhibits very little dependence on the doping concentration. When the doping concentration is increased above $10^{17}\ cm^{-3}$, however, the peak electron drift velocity diminishes.The peak electron drift velocity decreases from about $3.8x10^7 cm/s$ at $10^{16}cm^{-3}$ doping to around $3.5x10^7\ cm/s$ at $10^{19}\ cm^{-3}$ doping. The saturation electron drift velocity only drops slightly, however, from about $1.5x10^7\ cm/s$ at $10^{16}\ cm^{-3}$ doping to around $1.3x10^7\ cm/s$ at $10^{19}\ cm^{-3}$ doping. The low-field electron drift mobility, however, drops significantly with doping, from about $3400\ cm^2/Vs$ at $10^{16}cm^{-3}$ doping to around $1900\ cm^2/Vs$ at $10^{19}\ cm^{-3}$ doping at 300 K. The decrease in drift mobility with temperature at low fields is due to increased intravalley polar optical phonon scattering whereas the decrease in velocity at higher fields is due to increased intra and intervalley scattering.

It can be seen from the figure that the peak velocity also decreases and moves to higher electric field as the temperature is increased. This is due to the general increase of total scattering rate with temperature, which suppresses the electron energy and reduces the population of the satellite valleys.
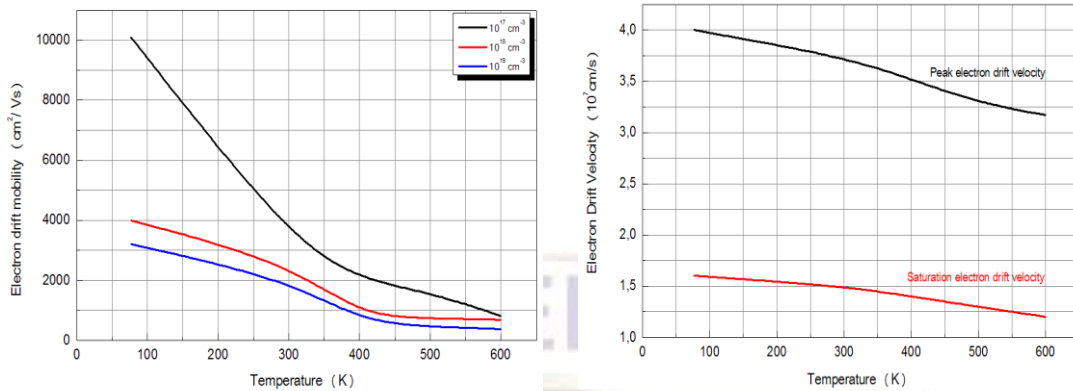
Fig.5. The low field electron drift mobility, the peak electron drift velocity and the saturation electron drift velocity associated with wurtzite InN as functions of the crystal temperature

This latter effect is apparent from the fact that the electron population in the central Γ valley increases with temperature.The peak electron drift velocity, the saturation electron drift velocity, and the low-field electron drift mobility associated with InN are plotted as functions of the crystal temperature in **Fig. 5**. The peak electron drift velocity, which is about $4x10^7 cm/s$ at $77\ K$, only decreases to around $3.2x10^7\ cm/s$ at $600\ K$. Similarly, the saturation electron drift velocity, which is about $1.6x10^7\ cm/s$ at $77\ K$, only decreases to around $1.2x10^7\ cm/s$ at $600\ K$. The low-field electron drift mobility associated with InN also diminishes in response to increases in the crystal temperature, from about $10000\ cm^2/Vs$ at 77 K to around $800\ cm^2/Vs$ at $600\ K$. The velocity-field characteristic associated with bulk wurtzite InN for various selections of the lowest conduction band valley effective mass, $m*$ are plotted in **Fig. 6**.
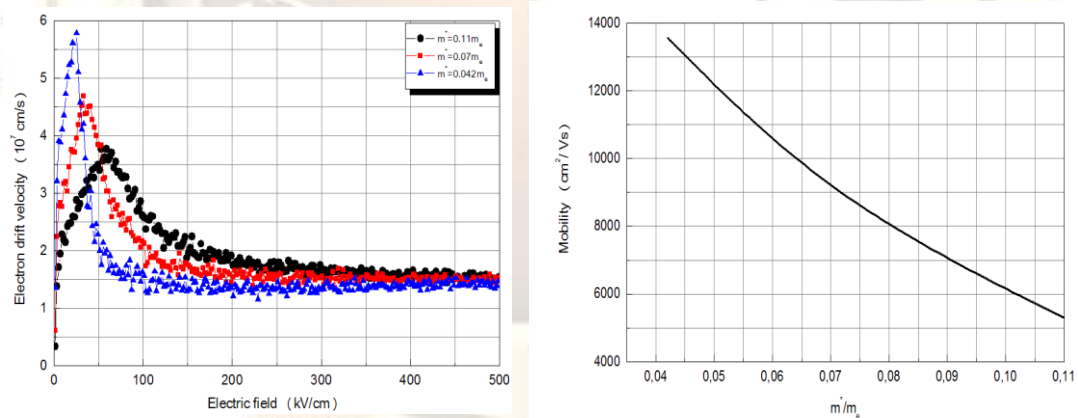
Fig.6. The velocity-field characteristic associated with bulk wurtzite InN for various selections of the lowest conduction band valley effective mass, $m*$

We note that this characteristic varies considerably in response to changes in $m*$. it is seen that the peak in the velocity-field characteristic lowers, broadens, and shifts to higher electric fields as $m*$ is increased. The peak electron drift velocity decreases from about $5.9x10^7 cm/s$ when $m*$ is set to 0.042 me to around $3.8x10^7 cm/s$ when $m*$ is set to $0.11m_e$. We note, however, that the saturation electron drift velocity decreases dramatically with increased m_u^*. The electric field at which the peak in the velocity-field characteristic occurs, here after referred to as the peak field, is seen to increase with $m*$, varying from about $24kV/cm$ when $m*$ is set to 0.042 me to around $68\ kV/cm$ when $m*$ is set to $0.11m_e$. The low-field electron drift mobility associated with InN are plotted as functions of the lowest conduction band valley effective mass, $m*$ in **Fig. 6**. We note that the low-field electron drift mobility decreases clearly as $m*$ is increased. In particular, the low-field electron drift mobility is found to decrease from about $13500\ cm^2/Vs$ when $m*$ is set to $0.042\ m_e$ to around $5300\ cm^2/Vs$ when $m*$ is set to $0.11\ m_e$.

**C.SAYAH, B.BOUAZZA, A.GUEN-BOUAZZA, N.E.CHABANE-SARI/ International
Journal of Engineering Research and Applications (IJERA)   ISSN: 2248-9622
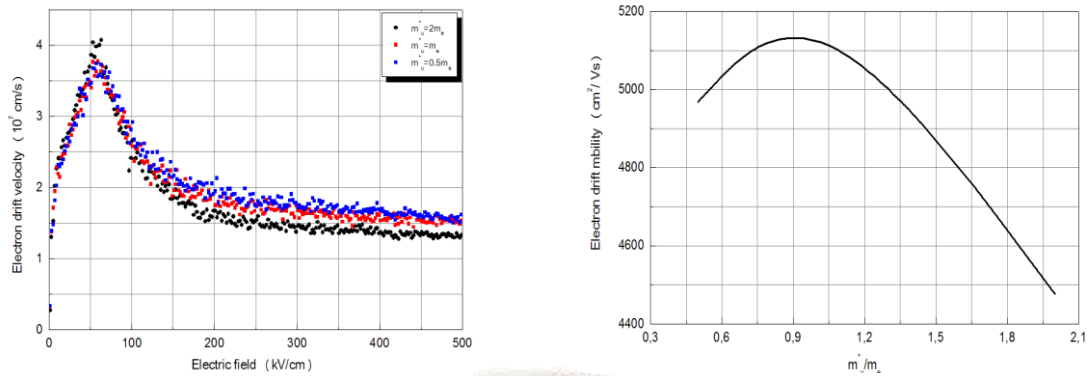www.ijera.com Vol. 2, Issue 1,Jan-Feb 2012, pp.476-482**

Fig.7. The velocity-field characteristic associated with bulk wurtzite InN for various selections of upper conduction band valley effective mass m_u^*

We now consider how changes in the upper conduction band valley effective masses, m_u^*, influence the velocity-field characteristic. In **Fig. 7**, we plot the velocity-field characteristic associated with bulk wurtzite InN for various selections of upper conduction band valley effective mass. In particular, we find that the saturation electron drift velocity decreases from about $1.7x10^7$ cm/s when m_u^* is set to $0.5m_e$ to around $1.2x10^7$ cm/s when m_u^* is set to $2m_e$. In contrast, the peak electron drift velocity and the peak field are found to be relatively insensitive to variations in m_u^*. The low-field electron drift mobility is around 5300 cm2/Vs when m_u^* is set to m_e.
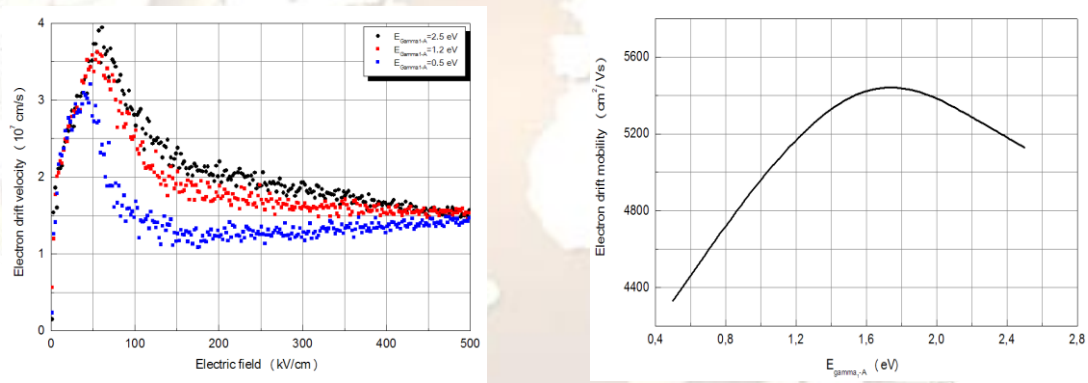

Fig.8. The velocity-field characteristic associated with bulk wurtzite InN for various conduction band intervalley energy separations E_{Γ_1-A}.

In **Fig. 8**, we study how the velocity-field characteristic associated with bulk wurtzite InN varies in response to changes in the conduction band intervalley energy separation E_{Γ_1-A}.
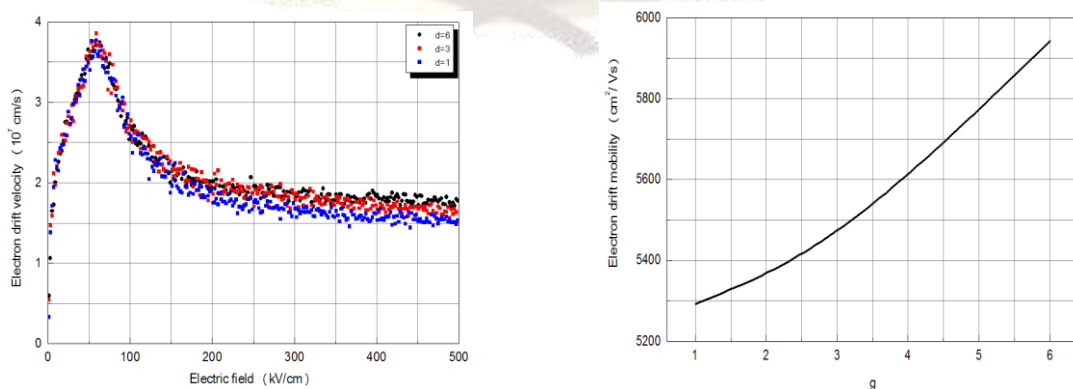

Fig.9. The velocity-field characteristic associated with bulk wurtzite InN for various upper conduction band valley degeneracy selections g

We note that the velocity-field characteristic associated with InN varies moderately when E_{Γ_1-A} is increased. We see that the peak electron drift velocity increases from about $3.1x10^7\ cm/s$ when E_{Γ_1-A} is set to 0.5 eV to around $3.8x10^7 cm/s$ when E_{Γ_1-A} is set to 2.2 eV. The peak field is also seen to increase monotonically with E_{Γ_1-A} increasing from about 50kV/cm when E_{Γ_1-A} is set to 0.5 eV to around 68 kV/cm when E_{Γ_1-A} is set to 2.2 eV. The low-field electron drift mobility being about 5300 cm2/Vs when E_{Γ_1-A} is set to 2.2 eV. In **Fig. 9**, we plot the velocity-field characteristic associated with bulk wurtzite InN for various upper conduction band minima degeneracy selections. The saturation electron drift velocity is found to be moderately sensitive to variations in the degeneracy. Quantitatively, we find that the saturation electron drift velocity decreases from about $1.8x10^{\ 7} cm/s$ when the degeneracy is set to one to around $1.3x10^{\ 7} cm/s$ when the degeneracy is set to six. The peak electron drift velocity and the peak field are seen to be relatively insensitive to the degeneracy. We note that the low-field electron drift mobility increases clearly as g is increased. In particular, the low-field electron drift mobility is found to increase from about $5300\ cm^2/Vs$ when g is set to 1 to around $5950\ cm^2/Vs$ when g is set to 6.

III. CONCLUSION

In conclusion, we have studied electron transport in InN using an ensemble Monte Carlo approach. Steady-state electron transport was the dominant theme of our analysis. We find that Indium Nitride exhibits a room temperature, steady-state peak drift velocity of around $3.8 \times 10^7\ cm/s$ at a doping concentration of $10^{16}\ cm^{-3}$, the corresponding saturation drift velocity being around $1.5 \times 10^7\ cm/s$. The sensitivity of these steady-state results to variations in temperature, doping concentration and the band structure parameters is examined. Monte Carlo simulation results showed that polar optical phonon scattering plays the dominant role in accounting for these differences in behavior. Bulk InN already had much better characteristics than GaN and AlN with regard to peak drift velocity and low-field mobility even when the traditionally accepted parameters are used. With the newly presented values it has superior characteristics with regard to these properties over the other materials.

IV. REFERENCES

[1] V.Yu. Davydov, A.A. Klochikhin, R.P. Seisyan, V.V. Emtsev, S.V. Ivanov, F. Bechstedt, J. Furthmuller, H. Harima, A.V. Murdryi, J. Aderhold, and O. Semchinova, J. Graul. Phys. Stat. Sol. (b) 229, R1 (2002).
[2] P. Carrier and S.-H. Wei, J. Appl. Phys. 97, 033707 (2005).
[3] J. Wu, W. Walukiewicz, K.M. Yu, J.W. Ager III, E.E. Haller, H. Lu, W.J. Schaff, Y. Saito, and Y. Nanishi, Appl. Phys. Lett. 80, 4741 (2002).
[4] I. Vurgaftman and J.R. Meyer, J. Appl. Phys. 89, 5816 (2001).
[5] I. Vurgaftman and J.R. Meyer, J. Appl. Phys. 94, 3675 (2003).
[6] B.R. Nag, Phys. Stat. Solidi (b) 237, R1 (2003).
[7] B. Arnaudov, T. Paskova, P.P. Paskov, B. Magnusson, E. Valcheva, B. Monemar, H. Lu, W.J. Schaff, H. Amano, and I. Akasaki, Phys. Rev. B 69, 115216 (2004).
[8] Q.X. Guo, T. Tanaka, M. Nishio, H. Ogawa, X.D. Pu, and W.Z. Shen, Appl. Phys. Lett. 86, 231913 (2005).
[9] S. Strite and H. Morkoc˛, J. Vac. Sci. Technol. B 10, 1237 (1992).
[10] C. Wetzel, T. Takeuchi, S. Yamaguchi, H. Katoh, H. Amono, and I. Akasaki, Appl. Phys. Lett. 73, 1994 (1998).
[11] W. Liang, K.T. Tsen, D.K. Ferry, H. Lu, and W.J. Schaff, Appl. Phys. Lett. 84, 3681 (2004).
[12] E. Bellotti, B.K. Doshi, and K.F. Brennan, J. Appl. Phys. 85, 916 (1999).
[13] W. Walukiewicz, S.K. Li, J. Wu, K.M. Yu, J.W. Ager III, E.E. Haller, H. Lu, and W.J. Schaff, J. Cryst. Growth 269, 119 (2004).
[14] B.R. Nag, J. Cryst. Growth 269, 35 (2004).
[15] C.H. Swartz, R.P. Tomkins, T.H. Myers, H. Lu, and W.J. Schaff, Phys. Status Solidi (c) 2, 2250 (2005).
[16] V.M. Polyakov and F. Schwierz, Appl. Phys. Lett. 88, 032101 (2006).
[17] B.E. Foutz, S.K. O_Leary, M.S. Shur, and L.F. Eastman, J. Appl. Phys. 85, 7727 (1999).
[18] S.K. O_Leary, B.E. Foutz, M.S. Shur, and L.F. Eastman, Appl. Phys. Lett. 87, 222103 (2005).
[19] C. Bulutay and B.K. Ridley, Superlattices Microstruct. 36, 465 (2004).
[20] Y.C. Yeo, T.C. Chong, and M.F. Li, J. Appl. Phys. 83, 1429 (1998).
[21] W.J. Fan, M.F. Li, T.C. Chong, and J.B. Xia, J. Appl. Phys. 79, 188 (1996).
[22] S. K. O'Leary, B. E. Foutz, M. S. Shur, L. F. Eastman, J Mater Sci: Mater Electron (2006) 17: 87–126, DOI 10.1007/s10854-006-5624-2
[23] Z. Yarar, B. Ozdemir, and M. Ozdemir, Journal of ELECTRONIC MATERIALS, Vol. 36, No. 10, 2007, DOI: 10.1007/s11664-007-0210-9